Published in final edited form as:
Biochemistry. 2006 April 11; 45(14): 4569–4577. doi:10.1021/bi052574s.

Effect of Site-directed Mutagenesis of Methylglyoxal- Modifiable Arginine Residues on the Structure and Chaperone Function of Human αA-crystallin

Ashis Biswas‡, **Antonia Miller**‡, **Tomoko Oya-Ito**‡, **Puttur Santhoshkumar**||, **Manjunatha Bhat**⊥, and **Ram H. Nagaraj**‡,§

‡ *Departments of Ophthalmology, Case Western Reserve University, Cleveland, OH 44106*

§ *Pharmacology, Case Western Reserve University, Cleveland, OH 44106*

⊥ *Center for Anesthesiology Research, Cleveland Clinic Foundation, Cleveland, OH 44195*

|| *Mason Eye Institute, University of Missouri, Columbia, MO 65212*

Abstract

We reported previously that chemical modification of human αA-crystallin by a metabolic dicarbonyl compound, methylglyoxal (MGO), enhances its chaperone-like function, a phenomenon which we attributed to formation of argpyrimidine at arginine residues (R) 21, 49 and 103. This structural change removes the positive charge on the arginine residues. To explore this mechanism further, we replaced these three R residues with a neutral alanine (A) residue one at time or in combination and examined the impact on the structure and chaperone function. Measurement of intrinsic tryptophan fluorescence and near-UV CD spectra revealed alteration of the microenvironment of aromatic amino acid residue in mutant proteins. When compared to wild type (wt) αA-crystallin, the chaperone function of R21A and R103A mutants increased 20% and 18% as measured by the insulin aggregation assay, and increased it as much as 39% and 28% when measured by the citrate synthase (CS) aggregation assay. While the R49A mutant lost most of its chaperone function, R21A/R103A and R21A/R49A/R103A mutants had slightly better function (6–14% and 10–14%) than the wt protein in these assays. R21A and R103A mutants had higher surface hydrophobicity than wt αA-crystallin, but the R49A mutant had lower hydrophobicity. R21A and R103A mutants, but not the R49A mutant, were more efficient than wt protein in refolding guanidine hydrochloride-treated malate dehydrogenase to its native state. Our findings indicate that the positive charges on R21, R49 and R103 are important determinants of the chaperone function of αA-crystallin and suggest that chemical modification of arginine residues may play a role in protein aggregation during lens aging and cataract formation.

Alpha-crystallin, a major structural lens protein in eyes of vertebrates, is a multimeric protein consisting of two subunits, αA- and αB-crystallin. These subunits usually combine in a in 3:1 ratio to form high molecular weight oligomers of ~ 800 kDa protein (1). The two proteins thus formed have approximately 60% amino acid sequence homology (2), and they belong to the small heat shock protein (sHSPs) superfamily (3,4). While αB-crystallin is found throughout the body, αA-crystallin is found primarily in the lens, although other tissues contain small quantities (5–7). Several years ago it was discovered that α-crystallin exhibits a molecular chaperone-like function (8,9). Like other sHSPs, α-crystallin prevents aggregation of

For correspondence: Ram H. Nagaraj, Ph.D., Department of Ophthalmology, Case Western Reserve University, Wearn Building, Room 653, Cleveland, OH 44106, Tel: 216-844-1132, Fax:216-844-7962, e-mail: ram.nagaraj@case.edu.

denaturing proteins (10). Since α-crystallin in the lens does not turn over, post-translational modifications presumably accumulate during aging. Numerous studies over the past few years addressed the relationship between various post-translational modifications and the chaperone function of α-crystallin. Investigators found that post-translational modifications such as, oxidation (11), phosphorylation (12), deamidation (13), and glycation (14,15) decreased the chaperone function of α-crystallin. Furthermore, the decreased chaperone function of α-crystallin was thought to cause protein aggregation during aging and cataract formation.

Glycation of α-crystallin is a major post-translational modification process in the lens. The reaction begins with condensation of the carbonyl function on carbohydrates, such as sugars and ascorbate oxidation products, with an amino group of proteins (on lysine and or N-terminal amino acid) to form a reversible Schiff base. This derivative then undergoes rearrangement to form a relatively stable Amadori product, *i.e.* ketoamine. Through a series of reactions, this product forms stable adducts on proteins that are collectively known as advanced glycation end products or AGEs (16). AGEs form as protein cross-linking adducts or non-cross-linking adducts, and they can be chromophoric and fluorophoric in nature. AGEs accumulate in lenses during the aging process, and they accumulate even more rapidly in cataractous lenses (17–19).

Recent studies suggest that α-dicarbonyl compounds, such as methylglyoxal (MGO) and glyoxal (GO), are major sources of AGEs in tissues (20). MGO is derived mostly from triose phosphate intermediates of glycolysis by non-enzymatic mechanisms (21). GO is derived from oxidation of several products, including, sugars, ascorbate and glycation intermediates (21). The human lens has higher concentrations of MGO than plasma (22). MGO is a highly reactive dicarbonyl compound. It reacts with arginine, lysine and cysteine residues in proteins (23). Several modifications of MGO have been detected in the lens, including hydroimidazolones (24,25) argpyrimidine (18,26), methylglyoxal-lysine dimer (MOLD) (27–29) and methylglyoxal 2-ammonio-6-([2-[(4-ammonio-5-oxido-5-oxopentyl) amino]-4-methyl-4,5-dihydro-1H-imidazol-5-ylidene]amino)hexanoate (MODIC) (30). Quantification of these products shows that MGO-modifications accumulate in cataractous lenses to a greater extent than in non-cataractous clear lenses (31). One recent study reported several micromolar hydroimidazolones per mg protein in the human lens (24), making them one of the major chemical modifications of lens proteins during aging and catactogenesis.

Amid these seemingly harmful effects of MGO, we made the surprising observation that when MGO reacts with αA-crystallin, it enhances its chaperone function (32). We then found that Hsp27, a related sHSP, also becomes a better chaperone and a better anti-apoptotic protein after modification by MGO (32). Our studies on αA-crystallin suggested that argpyrimidine modification by MGO is the most likely reason for the enhanced chaperone function, although hydroimidazole modifications may also bring about a similar effect. Using mass spectrometric analysis of the MGO-modified αA-crystallin, we identified three arginine residues, R21, R49 and R103 that were modified by argpyrimidine. Based on these findings, we reasoned that neutralization of the positive charge on the guanidine group of these arginine residues by argpyrimidine modification might result in enhanced chaperone function. In fact, data derived from experiments with several arginine modifying agents supports this interpretation (32). A few arginine mutations were previously identified in α-crystallin, but they decreased chaperone function and resulted in cataract formation (33). Those particular mutations occurred on arginine residues distinct from the MGO-modifiable ones. We interpret these findings to mean that mutations and argpyrimidine formation occur on different arginine residues and that they have opposite effects on the chaperone function of human αA-crystallin. To confirm our hypothesis, we generated a series of single and double mutants and one triple mutant of αA-crystallin in which we replaced MGO-modifiable arginine residues (R21, R49 and R103) with neutral alanine. We report the effect of these mutations on αA-crystallin structure and its

chaperone function and show that such changes provide a basis for the enhanced chaperone function by MGO modification.

EXPERIMENTAL PROCEDURES

Materials

Dithiothreitol (DTT), bovine insulin, malate dehydrogenase (MDH), carbonic anhydrase (CA), citrate synthase (CS), oxaloacetic acid and NADH were obtained from Sigma Chemical Co., St. Louis, MO. Citrate synthase was dialyzed against 40 mM HEPES buffer, pH 7.4 for 24 hrs before use. The reagent 2-*p*-toluidinylnaphthalene-6-sulphonate (TNS) was obtained from Molecular Probes (Invitrogen, Carlsbad, CA). Centrifugal filters (100 kDa cut off) centrifugal filters were obtained from Millipore (Bedford, MA). All other chemicals were of analytical grade.

Cloning and site directed mutagenesis

An N-terminal His tag and an enterokinase site were introduced into by PCR amplification into wt αA-crystallin harbored in a pET23d vector (kindly provided by Mark Petrash, Washington University, St Louis, MO). The PCR reaction contained 10 ng of wt αA-crystallin pET23d as template, 1 μM of forward primer (5′-CATGCCATGGGGCACCACCACCACCACCAC GATGA CGACGA CAAG- ATG GACGTGACCATCCAGCAC-3′) and reverse primer (5′-CCCAAGCTTAGGACG- AGGGAGCCGAGGT-3′), 200 μM dNTP and 2.5 U Pfu Turbo (Stratagene). PCR conditions were as follows: 95°C 5 min (1 cycle); 94 °C 1 min, 50°C 1 min, 72 °C 1 min, 72°C 1 min (36 cycles); 72°C 10 min (1 cycle). The 560 base pair PCR product was then cloned into pET23d between *Nco*I and *Hind*III restriction sites using a Takara DNA ligation kit according to the manufacturer's instructions (Takara, Shiga, Japan).

AlphaA-crystallin containing the R21A mutation was generated by PCR amplification from the wt αA-crystallin in pET23d vector using the forward primer indicated in Table 1 and the same reverse primer used to generate His-tagged wt αA-crystallin (see above). The resulting PCR product containing the mutation was then used in a second PCR reaction as the mega reverse primer; the forward primer was the same as that used to generate His-tagged wt αA-crystallin. The 560 base pair PCR product encoding the R21A mutant αA-crystallin was purified, digested and ligated into pET23d as described above. R49A, R103A, R21A/R49A, R21A/R103A and R21A/R49A/R103A mutants of αA-crystallin were generated by a similar method, using PCR amplification and either His tagged wt αA-crystallin or R21A αA-crystallin as templates and appropriate mutant primers (Table 1). Wt and mutant cDNA sequences were confirmed by restriction and DNA sequence analyses.

Protein purification

E. coli BL21(DE3)pLysS were transformed with plasmids containing either wt or mutant αA-crystallin cDNA. Expression of wt and mutant proteins were as follows: 500 ml of LB supplemented with ampicillin (100 μg/ml) was inoculated with 50 ml of an overnight culture of *E. coli* BL21(DE3)pLysS harboring the appropriate vector, and cultured at 37 °C, 250 rpm, until the optical density (O.D.) was 0.5 - 0.7. Induction of α-crystallin expression was initiated by addition of 250 μM IPTG. The cultures were then grown 4–5 hrs longer at 37 °C, and the cells were harvested by centrifugation at 5,000 *x* g for 10 minutes at 4 °C. Pellets were resuspended in 5 ml/g of lysis buffer (100 mM NaH_2PO_4, 10 mM Tris, 8M urea, pH 8) and gently mixed for 1 hr at room temperature. Lysates were immersed in ice and dispersed by 3 × 40 second bursts of sonication at 40 % amplitude using a Branson Digital Sonifier (Danbury, CT). All samples were centrifuged at 12,000 × *g* for 30 minutes. Each lysate was incubated with the appropriate amount of Ni-NTA resin according to the manufacturer's instructions (Qiagen, Valencia, CA) and gently mixed for 1 hour at room temperature before loading onto

a prepared column. The columns were washed with buffer (pH 7.0) containing 100 mM NaH_2PO_4, 10 mM Tris, 8M urea, and eluted with the same buffer at pH 5.5. The fractions were separated by SDS-PAGE, and immunoreactivity was assessed by Western blotting with an antibody to αA/αB-crystallin as described below. Proteins that appeared as a single band at 20 kDa were pooled and extensively dialyzed at 4°C against 50 mM Tris-HCl (pH 8.0). The pooled protein was then concentrated using Amicon Ultra-15 centrifugal filters (Millipore) and stored at −20 °C.

SDS-PAGE and Western blotting

4 μg of protein and Precision Protein Standard (Bio-Rad Laboratories, Hercules, CA) were loaded onto two 12% SDS-PAGE gels and subjected to electrophoresis at 150V for 1.5 hrs. After this time, one gel was stained with Bio-Safe Coomassie (Bio-Rad), and protein from the other was transferred electrophoretically to a nitrocellulose membrane (100 V for 1 hr). The membrane was blocked by overnight incubation at 4°C in buffer A (5% NFDM in PBS). The blocked membrane was then incubated with polyclonal rabbit anti-αA/αB–crystallin antibody in buffer A (1:3,000) (Stressgen, Victoria, BC, Canada) at room temperature for 1 hr. Following this initial incubation, the membrane was washed extensively with 0. 05% Tween-20 in PBS and incubated for 1 hr at room temperature with a 1:3000 dilution of HRP-conjugated goat-anti-rabbit IgG (Sigma) in 0.05% Tween-20 in PBS along with 1:10000 diluted Precision StrepTacin-HRP conjugate (Bio-Rad). The membrane was again washed extensively with 0.05% Tween-20, developed with SuperSignal West Pico Chemiluminescent stain (Pierce, Rockford, IL) and photographed.

Determination of molecular mass by dynamic light scattering

We used dynamic light scattering measurements to determine the molar mass of the wild type and mutant proteins as described earlier (34). In brief, purified recombinant proteins were incubated at 37°C for 1 hr and then chromatographed on a TSK G5000PW_{XL} (Tosoh Bioscience, Inc., San Francisco, CA) size-exclusion column using phosphate buffer (0.05 M + 0.3 M NaCl, pH 7.2). The column was connected to an HPLC fitted with an RID detector (Shimadzu) and coupled to multi-angle light scattering (DAWN) and Quasi Elastic Light Scattering detectors (Wyatt Technology Corp., Santa Barbara, CA). Molar mass (M_w), polydispersity index (PDI) and hydrodynamic radius (R_h) of the samples were determined using ASTRA (5.1.5) software developed by Wyatt Technology Corp.

Circular dichroism (CD) measurements

The conformation of αA-crystallin was examined by recording far-UV and near-UV CD spectra at 25 °C in a Jasco 810 spectropolarimeter (Jasco, Inc., Japan) flashed with dry nitrogen. The far-UV CD spectra were collected from 250 to 195 nm in a CD quartz cell of 1 mm path length using a slit width of 1 nm and a scan speed 20 nm/min. The reported spectra, the average of 5 scans, were analyzed for secondary structure by the curve fitting program CONTINLL (35). Far-UV CD spectra were recorded from 0.2 mg/ml proteins in 10 mM phosphate buffer (pH 7.2). Near-UV CD spectra were recorded from 1 mg/ml protein in the same phosphate buffer. Spectra were collected from 300 to 250 nm using a CD cell of 10 mm path length.

Tryptophan fluorescence measurements

The intrinsic tryptophan fluorescence spectrum of αA-crystallin at 25 °C was recorded in a Varian Eclipse spectrofluorometer (Varian Inc., CA). Fluorescence emission spectrum of each protein (0.1 mg/ml) in 50 mM phosphate buffer (pH 7.2) was recorded between 310–400 nm using 295 nm as the excitation wavelength. The excitation and emission band passes were 5 nm each.

TNS fluorescence measurements

The surface hydrophobicity of the wild type and mutant human αA-crystallin was studied with TNS, a specific hydrophobic probe. Ten μl of 10 mM methanolic solution of TNS was added to 1 ml protein (0.1 mg/ml in 50 mM phosphate buffer (pH 7.4), and the mixture was incubated for 2 hrs at 25 °C. Fluorescence emission spectra were recorded between 350–520 nm using an excitation wavelength of 320 nm. The excitation and emission band passes were 5 nm each.

Chaperone-like function of wild type and mutant human aA-crystallin

The chaperone-like function was determined with three target proteins: insulin, citrate synthase (CS) and carbonic anhydrase (CA). For insulin and CS, chaperone activity was assayed in 96-microwell plates using a microplate reader (Molecular Devices, SpectraMax, Model 190, Sunnyvale, CA). The total reaction volume was 250 μl.

(a) Insulin aggregation assay—Insulin (0.32 mg/ml) in 50 mM phosphate buffer (pH 7.2) was incubated at 25 °C with or without wild type (wt) or mutant αA-crystallin (0.064 mg/ml). Insulin aggregation was initiated by adding freshly prepared DTT to a final concentration of 20 mM, and light scattering at 400 nm was monitored for 1 hr in the kinetic mode (36).

(b) CS aggregation assay—CS (0.06 mg/ml in 40 mM HEPES buffer, pH 7.4) was incubated in presence or absence of different αA-crystallin preparations at 43 °C, and light scattering was monitored at 360 nm (37). The ratio of α-crystallin to CS was 1:15 (w/w).

(c) CA aggregation assay—Six hundred μl of CA (0.24 mg/ml) in 50 mM phosphate buffer containing 100 mM NaCl (pH 7.2) was incubated at 60°C with or without wt or mutant αA-crystallins (0.06 mg/ml) in a Beckman DU spectrophotometer (Fullerton, CA). Light scattering at 400 nm was monitored for 1 hr in a kinetic mode.

Determination of binding parameters between carbonic anhydrase (CA) and αA-crystallin

Wild type or mutant αA-crystallin (12.5 μM) was incubated at 60 °C for 1 hr with 2–18 μM CA in 50 mM phosphate buffer containing 100 mM NaCl (pH 7.2). No protein aggregation was observed under these conditions. The solutions were cooled to 25 °C for 1 hr. Unbound substrate was then separated by centrifugation at 4,000 *x* g through 100 kDa cut off membrane filters. The amount of remaining substrate (CA) associated with α-crystallin was calculated by subtracting free substrate from the total substrate concentration. Protein concentrations were determined by the Bradford assay using BSA as the standard. The number of binding sites (n) and dissociation constant (K_d) were determined by a similar procedure (38).

Protein refolding assay

Chaperone efficiency was also assessed by measuring the α-crystallin-mediated refolding of a homodimeric enzyme, malate dehyrogenase (MDH), from its fully unfolded state. MDH (1 μM) was denatured in 6M Gu-HCl for 8 hrs at 25 °C. Refolding of the enzyme was initiated by diluting the denatured MDH 100-fold in a refolding buffer (pH 7.5) containing 50 mM phosphate, 10 mM magnesium acetate, 5 mM DTT, with or without the addition of 30 μM αA-crystallin. The enzyme concentration was 10 nM during refolding. The activity of refolded enzyme was assayed by adding 20 μl of refolding mixture to 580 μl of refolding buffer that also contained 0.1 mM NADH and 0.4 mM oxaloacetate. The samples were pre-incubated at 25°C for 10 min and the decrease in absorbance at 340 nm with time was recorded.

RESULTS AND DISCUSSION

In our previous study (32), we discovered that modification of αA-crystallin by MGO resulted in enhanced chaperone function, and we found that this phenomenon depended upon the concentration of MGO. Based on immunoprecipitation experiments with a monoclonal antibody against argpyrimidine and mass spectrometric analysis of the protein, we reasoned that argpyrimidine modification at R21, R49 and R103 of αA-crystallin could explain the enhanced chaperone function. It is possible that hydroimidazolone modifications at these sites might also result in enhanced chaperone function. Soon after our discovery, another study confirmed that chaperone function of α-crystallin is improved by MGO modification (39). Furthermore, another recent study reported enhanced chaperone function of α-crystallin when a nine amino acid peptide at the N-terminus harboring R21 residue was deleted (40). Taken together these observations indicate that the positive charge on specific arginine residues influences the chaperone function of α-crystallin. To further investigate the role of these MGO-modifiable arginine residues in α-crystallin, we used site directed mutagenesis to replace arginine residues at positions 21, 49 and 103 with neutral alanine residues. Even though neutralization of positive charge on arginine residues appears to be the major factor, we cannot exclude changes in physical properties such as, van der Waals interaction and dipole moment and other factors such as, hydrophobicity and nucleophilicity contributing to the improvement in the chaperone function of αA-crystallin.

We prepared six mutants of human αA-crystallin: R21A, R49A, R103A, R21A/R49A, R21A/R103A and R21A/R49A/R103A as described above (Experimental Procedures). For over-expression, plasmids of wild type and mutant human αA-crystallins were introduced into *E. coli* strain BL21(DE3)pLysS. Protein expression was induced by the addition of IPTG. Bacterial cell pellets were solublilized by sonication in phosphate buffer containing 100 mM Na_2HPO_4, 10 mM Tris-HCl (pH 8). This procedure yielded significant quantities of soluble wt protein, but it proved ineffective for solubilizing the mutant proteins. Since we were able to solubilize both wt and mutant proteins by sonication in the presence of 8M urea, we used this procedure in our purification protocol. SDS-PAGE and Western blotting showed single bands, indicating that this method yielded pure proteins (Fig. 1).

Multi-angle light scattering coupled with size exclusion chromatography determines polydispersity and estimates the absolute molar mass and size, which cannot be obtained by conventional chromatographic detection methods (41). Accordingly, we compared the quaternary structure, *i.e.* oligomeric size and molecular mass of wt and mutant proteins, by the dynamic light scattering method. Table 2 shows the estimated oligomeric sizes of various proteins. The average molar mass (M_w) and hydrodynamic radii (R_h) value of wt αA-crystallin suggest that it has a higher oligomeric size than the reported value (42,43). The large oligomeric size of the wt protein may be due to its purification in the presence of urea. We noted that all mutants except R21A exhibited a wider mass distribution, and all except R21A and R21A/R103A had a M_w compared to the wt protein. The R21A mutation rendered αA-crystallin less polydisperse, while R49A and R103A made it more polydisperse (Table 2). This suggests that R21, R49 and R103 residues have a role in αA-crystallin organization. Because all other mutants (except R21A) had higher hydrodynamic radii (R_h) values, we believe that they are less dynamic than wt protein. Overall, our findings suggest that the removal of the positive charge from R49 and R103 results in higher molecular weight homoaggregates of αA-crystallin. This is similar to observations made for the two arginine mutants, R116C in αA- and R120G in αB-crystallin, where it was noted that arginine residues at these positions are essential for maintaining proper oligomeric structure (44,45).

We probed the secondary structure of wt and mutant αA-crystallins by far-UV circular dichroism. All the spectra reflect characteristics of dominant β-sheet structure. The spectra

were quantitatively analyzed using the CONTINLL program. The estimated levels of secondary structure are listed in Table 3. The values suggest that there is no significant change in the secondary structure in any of the mutant proteins. We also studied the effect of mutation on the secondary structure using fourier-transform infrared spectroscopy (data not shown). The data confirmed the results from far UV measurements indicating that our selected mutations did not perturb the secondary structure of proteins.

The near UV CD spectra of the six mutants and wt αA-crystallin are shown in Fig. 2. The near UV spectrum of wt protein exhibited five distinct maxima (around 259, 264, 272, 279 and 287 nm) and five distinct minima (around 262, 268, 275, 283 and 292 nm), which is consistent with previously published results (46). The signal for Phe in the 250–270 nm region showed minimal alteration in the six mutants compared to the wt protein. However, peaks beyond 270 nm for all six mutants were significantly different both in intensity and position from those for wt protein. These marked changes in spectral characteristics of six mutants suggest alteration of the microenvironments of Tyr and/or Trp and indicate that the tertiary structure of the mutant proteins could be changed by substitution of alanine for the charged arginine residues.

Intrinsic fluorescence spectra of the wt and mutant αA-crystallins (Fig. 3) support our near-UV CD data. While the fluorescence intensity of R49A, R21A/R49A and R21A/R49A/R103A decreased ~ 12–14% compared to the wt protein, it increased slightly in R21A, R21A/R103A and R103A. Alteration in fluorescence emission maxima was also noticeable. The fluorescence emission maximum (λ_{max}) of wt αA-crystallin was at 344 nm. We found that the λ_{max} of six mutants exhibited ~2 nm blue shift, which suggests that the tryptophan microenvironment is somewhat altered in all mutant proteins. These observations support our previous conclusions that minor structural changes enhance the chaperone function of αA-crystallin (32).

We explored the effect of structural changes on the chaperone-like activity of wt αA-crystallin and six mutant proteins using two target proteins, insulin and citrate synthase. Figure 4A shows the profile of DTT-induced insulin aggregation of in the presence or absence of wt and mutant αA-crystallins. At 1:5 (w/w) ratio of wt αA-crystallin to insulin and l hr incubation, we noted ~30% of protection against aggregation (Fig. 4A, trace 4and 4C). At the same protein ratio, R21A and R103A markedly increased chaperone function, providing 50% and 48% protection (4A, traces 7 and 8 and 4C). In contrast, R49A and R21A/R49A mutants decreased chaperone function and provided only ~11% and ~ 27% protection against insulin aggregation (Fig. 4A, traces 2 and 3 and 4C). The double mutant R21A/R103A and the triple mutant R21A/R49A/R103A afforded slightly better protection than wt αA-crystallin (Fig. 4C). With CS as the target protein, we saw a more dramatic effect. At a chaperone: substrate ratio of 1:15 (w/w), R49A (Fig. 4B, trace 2) and R21A/R49A (4B, trace 3) inhibited protein aggregation minimally. At the same ratio, R21A and R103A inhibited protein aggregation 39% and 28% better than wt αA-crystallin (Fig. 4B, traces 7 and 8 and 4D). We also compared the chaperone function of wt and six mutant proteins by varying the α-crystallin:substrate ratio. In each case, we found that the R21A and R103A mutants to be better than wt and R49A to be less effective than the wt in preventing aggregation of the target protein (data not shown). Taken together, these data suggest that a significant loss in chaperone function occurs when the positive charge on R49 is removed, but an opposite and favorable increase in chaperone function occurs with removal of positive charge on R21 and R103. The strength of the chaperone function decreases in the following order: R21A > R103A > R21A/R49A/R103A > R21A/R103A > wt > R21A/R49A > R49A. We believe that this is the first report of an increase in the chaperone function of α-crystallin due to removal of a single arginine residue without changes in the secondary structure detected by CD spectra and tryptophan fluorescence. We think that the improved chaperone function reported by Pasta et al (40) in deletion mutants of α-crystallin may be due to removal of the R21 residue from the N-terminal end of the protein.

Numerous studies suggested a correlation between chaperone function and surface exposed hydrophobicity in α-crystallin (38,47–50) but a few others failed to find such a correlation (51,52). Notwithstanding this controversy, it is generally believed that surface hydrophobicity governs the chaperone function of α-crystallin. Accordingly, we used TNS, a hydrophobic molecule (with low fluorescence quantum yield in water) to explore how mutation of arginine residues affects the hydrophobicity of αA-crystallin. When TNS binds to hydrophobic sites on proteins, its quantum yield dramatically increases (53). This dye has been widely used for probing the surface hydrophobicity of α-crystallin (13,44,54). Figure 5A shows fluorescence measurements of TNS after binding to wt and mutant αA-crystallins. Upon binding to the wt αA-crystallin TNS displays intense fluorescence with emission maximum (λ_{max}) at 430 nm. This λ_{max} did not change in mutant proteins. The results suggest that R21A and R103A both have ~55% more hydrophobic surface area compared to the wt αA-crystallin (Fig. 5A, B) and the triple mutant has ~20% more. In contrast, R49A and R21A/R49A mutant proteins had decreased (~26% and 18%) surface hydrophobicity (Figs. 5A and B). The surface hydrophobicity of our selected mutants decreased in the following order: R21A> R103A> R21A/R49A/R103A > R21A/R103A > wt > R21A/R49A > R49A (Fig. 5B). The decreasing order of the surface hydrophobicity coincides with decreasing chaperone function. From these results, we could conclude that the enhanced chaperone function of mutant proteins was due to increased surface hydrophobicity. However, this interpretation conflicts with the results of two previous studies, where MGO-mediated enhancement in chaperone function did not correlate with surface hydrophobicity of α-crystallin (32,39). Possibly MGO-modification (and ensuing cross-linking) of α-crystallin impedes the binding of hydrophobic probes.

In order to determine how the interaction between αA-crystallin and denaturing substrates would be affected by arginine mutations, we measured the binding parameters using carbonic anhydrase (CA) as the substrate. Before determining the binding constant and number of binding sites (n), we first compared the chaperone activity of wt and mutant αA-crystallin proteins using CA as the target protein. We used only three single mutants for these experiments. Fig. 6 shows the thermal aggregation profile of 0.24 mg/ml CA at 60 °C in the presence or absence of wt and mutant αA-crystallin (0.06 mg/ml). The chaperone function followed the same pattern as the insulin and CS aggregation assays, proceeding from highest to lowest in the following order: R21A > R103A > wt > R49A. To determine binding constants we incubated 12.5 μM of αA-crystallin at 60 °C for 1 hr with varying concentrations (2–18 μM) of CA. Unbound (S) and bound CA were measured by filtration as described above under Experimental Procedures. Assuming that there are identical non-interacting sites per subunit of the chaperone, the dissociation constant (K_d) was analyzed by Scatchard equation:

$$\tilde{\nu}/S = n/K_d - 1/K_d \cdot \tilde{\nu} \qquad \text{Eq. 1}$$

where $\tilde{\nu}$ is the number of moles of substrate bound per mole of chaperone, 'n' is the number of binding site and K_d is the dissociation constant. The stoichiometry n and K_d obtained from the plot of $\tilde{\nu}$/S against $\tilde{\nu}$ (Fig. 7) is 2.32 per subunit of αA-crystallin and 3.87 μM respectively (Table 4). When R21A interacts with CA, we found the number of binding sites (n) per subunit increased considerably (from 2.32 to 3.73) and the association constant increased from 0.258 μM^{-1} (K_d = 3.87 μM) to 0.342 μM^{-1} (K_d = 2.92 μM). The binding parameters for the interaction between CA and R103A also indicate enhanced CA binding. In contrast, we found that the number of binding sites (n) for CA on R49A decreased significantly (from 2.63 to 1.79), although the dissociation constant (K_d) for this interaction was quite similar to that of wt αA-crystallin. Based on these data, we conclude that substitution of alanine for charged arginine residues at positions 21 and 103 provides higher affinity toward denaturing proteins for αA-crystallin.

Alpha-crystallin also assists in the *in vitro* refolding of many enzymes (55–58). As a measure of this activity, we examined the ability of wt and mutant αA-crystallins to reactivate fully

denatured malate dehydrogenase (MDH). MDH was renatured by 100-fold dilution from 6M Gu-HCl to refolding buffer, and refolding was measured in the presence or absence αA-crystallin (Fig. 8). In the absence of αA-crystallin, only 3% activity was recovered (trace 5). In the presence of 30 μM wt αA-crystallin about 41% activity of MDH could be regained (trace 3). R21A and R103A mutant proteins at the same protein concentration provided a further increase of 9% and 4% (traces 1 and 2). As expected, the recovery of enzyme activity with R49A was drastically reduced (~13% less than with wt αA-crystallin) (trace 4). Thus, both aggregation and refolding activity assays show that mutation of charged R21 and R103 markedly enhance the chaperone function of αA-crystallin, while mutation of R49 decreases it.

We noted that the increase in chaperone function does not correspond quantitatively with enhanced surface hydrophobicity. For example, the R21A mutant protein enhanced hydrophobicity more than 55% but only increased refolding approximately 10% (Fig. 8, trace 1). The insulin aggregation assay for the same protein indicates ~ 20% increase in chaperone activity above that of the wt αA-crystallin (Fig. 4C). This anomaly could be explained if the hydrophobic probe, TNS, binds to all the exposed hydrophobic patches, but not all of them are accessible or large enough to accommodate the target protein.

The correlation between oligomeric size and chaperone function of α-crystallin is still unclear. Several previous studies showed that increased oligomeric size diminishes chaperone function (44,45), whereas others indicated the opposite, that greater oligomeric size enhances chaperone function (34,59). Our own studies failed to indicate a correlation between the oligomeric size and chaperone function of αA-crystallin. Because protein turnover within the lens is negligible, we speculate that oligomerization provides the structural stability necessary for α-crystallin to maintain its chaperone function for many years.

Our results suggest that each of the positive charges on R21, R103 and R49 sites in αA-crystallin are important for chaperone function. The R49A mutation seems to have a strong negative effect on the chaperone function, which was not overcome by inclusion of a R21A mutation, even though mutation at R21A alone significantly increased the chaperone function of αA-crystallin. The triple mutant, unlike the double mutant R21A/R49A, was a much better chaperone than the wt αA-crystallin, suggesting that mutation at R103A has the strongest positive effect on the chaperone function of αA-crystallin. The influence of R103A appears even greater than the R21A mutation.

Although reaction with MGO changes the charge on all three arginine residues, the overall effect is most likely a gain of function, as evident from the behavior of the triple mutant R21A/R49A/R103A. Our studies provide an explanation for the MGO-induced enhancement in chaperone function of αA-crystallin. It seems likely that MGO-induced changes help to maintain the chaperone function of α-crystallin during aging and cataractogenesis.

Acknowledgements

We thank Witold Surewicz, Michael Zagorski and Clemens Burda of Case Western Reserve University, Cleveland, OH for use of the FTIR, CD spectropolarimeter and the fluorescence spectrofluorometer. We are grateful to Dr. J. Mark Petrash, Washington University, St. Louis, MO for the human αA-crystallin-pET23d vector.

This study was supported from NIH grants R01EY-016219 and R01EY-09912 (RHN), P30EY-11373 (Visual Sciences Research Center of CWRU), Research to Prevent Blindness (RPB), NY and Ohio Lions Eye Research Foundation.

Abbreviations Used

sHSP

small heat shock protein

AGEs
advanced glycation end products

PMSF
phenyl methyl sulfonyl fluoride

DTT
dithiothreitol

IPTG
isopropyl-β-D-thiogalactoside

Gu-HCl
guanidine hydrochloride

CA
carbonic anhydrase

CS
citrate synthase

MDH
malate dehydrogenase

MGO
methylglyoxal

GO
glyoxal

TNS
2-(p-toludino) naphthalene-6-sulfonic acid, sodium salt

NADH
β-nicotinamide adenine nucleotide, reduced dipotassium salt

References

1. Spector A, Li LK, Augusteyn RC, Schneider A, Freund T. -Crystallin. The isolation and characterization of distinct macromolecular fractions. Biochem J 1971;124:337–43. [PubMed: 5158502]
2. Bloemendal H. Lens proteins. CRC Crit Rev Biochem 1982;12:1–38. [PubMed: 7037295]
3. de Jong WW, Caspers GJ, Leunissen JA. Genealogy of the alpha-crystallin--small heat-shock protein superfamily. Int J Biol Macromol 1998;22:151–62. [PubMed: 9650070]
4. de Jong WW, Leunissen JA, Voorter CE. Evolution of the alpha-crystallin/small heat-shock protein family. Mol Biol Evol 1993;10:103–26. [PubMed: 8450753]
5. Kapphahn RJ, Ethen CM, Peters EA, Higgins L, Ferrington DA. Modified alpha A crystallin in the retina: altered expression and truncation with aging. Biochemistry 2003;42:15310–25. [PubMed: 14690441]
6. Iwaki T, Kume-Iwaki A, Goldman JE. Cellular distribution of alpha B-crystallin in non-lenticular tissues. J Histochem Cytochem 1990;38:31–9. [PubMed: 2294148]
7. van Boekel MA, Hoogakker SE, Harding JJ, de Jong WW. The influence of some post-translational modifications on the chaperone-like activity of alpha-crystallin. Ophthalmic Res 1996;28(Suppl 1): 32–8. [PubMed: 8727961]
8. Horwitz J. Alpha-crystallin can function as a molecular chaperone. Proc Natl Acad Sci U S A 1992;89:10449–53. [PubMed: 1438232]
9. Horwitz J. Alpha-crystallin. Exp Eye Res 2003;76:145–53. [PubMed: 12565801]

10. Bloemendal H, de Jong W, Jaenicke R, Lubsen NH, Slingsby C, Tardieu A. Ageing and vision: structure, stability and function of lens crystallins. Prog Biophys Mol Biol 2004;86:407–85. [PubMed: 15302206]
11. Fujii N, Hiroki K, Matsumoto S, Masuda K, Inoue M, Tanaka Y, Awakura M, Akaboshi M. Correlation between the loss of the chaperone-like activity and the oxidation, isomerization and racemization of gamma-irradiated alpha-crystallin. Photochem Photobiol 2001;74:477–82. [PubMed: 11594064]
12. Ito H, Kamei K, Iwamoto I, Inaguma Y, Nohara D, Kato K. Phosphorylation-induced change of the oligomerization state of alpha B-crystallin. J Biol Chem 2001;276:5346–52. [PubMed: 11096101]
13. Gupta R, Srivastava OP. Deamidation affects structural and functional properties of human alphaA-crystallin and its oligomerization with alphaB-crystallin. J Biol Chem 2004;279:44258–69. [PubMed: 15284238]
14. Derham BK, Harding JJ. Alpha-crystallin as a molecular chaperone. Prog Retin Eye Res 1999;18:463–509. [PubMed: 10217480]
15. Cherian M, Abraham EC. Decreased molecular chaperone property of alpha-crystallins due to posttranslational modifications. Biochem Biophys Res Commun 1995;208:675–9. [PubMed: 7695622]
16. Baynes JW. The role of AGEs in aging: causation or correlation. Exp Gerontol 2001;36:1527–37. [PubMed: 11525875]
17. Nagaraj RH, Sell DR, Prabhakaram M, Ortwerth BJ, Monnier VM. High correlation between pentosidine protein crosslinks and pigmentation implicates ascorbate oxidation in human lens senescence and cataractogenesis. Proc Natl Acad Sci U S A 1991;88:10257–61. [PubMed: 1946446]
18. Wilker SC, Chellan P, Arnold BM, Nagaraj RH. Chromatographic quantification of argpyrimidine, a methylglyoxal-derived product in tissue proteins: comparison with pentosidine. Anal Biochem 2001;290:353–8. [PubMed: 11237339]
19. Lyons TJ, Silvestri G, Dunn JA, Dyer DG, Baynes JW. Role of glycation in modification of lens crystallins in diabetic and nondiabetic senile cataracts. Diabetes 1991;40:1010–5. [PubMed: 1907246]
20. Wells-Knecht KJ, Brinkmann E, Wells-Knecht MC, Litchfield JE, Ahmed MU, Reddy S, Zyzak DV, Thorpe SR, Baynes JW. New biomarkers of Maillard reaction damage to proteins. Nephrol Dial Transplant 1996;11(Suppl 5):41–7. [PubMed: 9044306]
21. Thornalley PJ. The glyoxalase system in health and disease. Mol Aspects Med 1993;14:287–371. [PubMed: 8277832]
22. Haik GM Jr, Lo TW, Thornalley PJ. Methylglyoxal concentration and glyoxalase activities in the human lens. Exp Eye Res 1994;59:497–500. [PubMed: 7859825]
23. Lo TW, Westwood ME, McLellan AC, Selwood T, Thornalley PJ. Binding and modification of proteins by methylglyoxal under physiological conditions. A kinetic and mechanistic study with N alpha-acetylarginine, N alpha-acetylcysteine, and N alpha-acetyllysine, and bovine serum albumin. J Biol Chem 1994;269:32299–305. [PubMed: 7798230]
24. Ahmed N, Thornalley PJ, Dawczynski J, Franke S, Strobel J, Stein G, Haik GM. Methylglyoxal-derived hydroimidazolone advanced glycation end-products of human lens proteins. Invest Ophthalmol Vis Sci 2003;44:5287–92. [PubMed: 14638728]
25. Thornalley PJ, Battah S, Ahmed N, Karachalias N, Agalou S, Babaei-Jadidi R, Dawnay A. Quantitative screening of advanced glycation endproducts in cellular and extracellular proteins by tandem mass spectrometry. Biochem J 2003;375:581–92. [PubMed: 12885296]
26. Shipanova IN, Glomb MA, Nagaraj RH. Protein modification by methylglyoxal: chemical nature and synthetic mechanism of a major fluorescent adduct. Arch Biochem Biophys 1997;344:29–36. [PubMed: 9244378]
27. Nagaraj RH, Sady C. The presence of a glucose-derived Maillard reaction product in the human lens. FEBS Lett 1996;382:234–8. [PubMed: 8605976]
28. Chellan P, Nagaraj RH. Protein crosslinking by the Maillard reaction: dicarbonyl-derived imidazolium crosslinks in aging and diabetes. Arch Biochem Biophys 1999;368:98–104. [PubMed: 10415116]

29. Ahmed MU, Brinkmann Frye E, Degenhardt TP, Thorpe SR, Baynes JW. N-epsilon-(carboxyethyl) lysine, a product of the chemical modification of proteins by methylglyoxal, increases with age in human lens proteins. Biochem J 1997;324(Pt 2):565–70. [PubMed: 9182719]
30. Biemel KM, Friedl DA, Lederer MO. Identification and quantification of major maillard cross-links in human serum albumin and lens protein. Evidence for glucosepane as the dominant compound. J Biol Chem 2002;277:24907–15. [PubMed: 11978796]
31. Padayatti PS, Ng AS, Uchida K, Glomb MA, Nagaraj RH. Argpyrimidine, a blue fluorophore in human lens proteins: high levels in brunescent cataractous lenses. Invest Ophthalmol Vis Sci 2001;42:1299–304. [PubMed: 11328743]
32. Nagaraj RH, Oya-Ito T, Padayatti PS, Kumar R, Mehta S, West K, Levison B, Sun J, Crabb JW, Padival AK. Enhancement of chaperone function of alpha-crystallin by methylglyoxal modification. Biochemistry 2003;42:10746–55. [PubMed: 12962499]
33. Kumar LV, Ramakrishna T, Rao CM. Structural and functional consequences of the mutation of a conserved arginine residue in alphaA and alphaB crystallins. J Biol Chem 1999;274:24137–41. [PubMed: 10446186]
34. Sreelakshmi Y, Sharma KK. Recognition sequence 2 (residues 60–71) plays a role in oligomerization and exchange dynamics of alphaB-crystallin. Biochemistry 2005;44:12245–52. [PubMed: 16142923]
35. Provencher SW, Glockner J. Estimation of globular protein secondary structure from circular dichroism. Biochemistry 1981;20:33–7. [PubMed: 7470476]
36. Bhattacharyya J, Das KP. Alpha-crystallin does not require temperature activation for its chaperone-like activity. Biochem Mol Biol Int 1998;46:249–58. [PubMed: 9801793]
37. Santhoshkumar P, Sharma KK. Phe71 is essential for chaperone-like function in alpha A-crystallin. J Biol Chem 2001;276:47094–9. [PubMed: 11598124]
38. Biswas A, Das KP. Role of ATP on the interaction of alpha-crystallin with its substrates and its implications for the molecular chaperone function. J Biol Chem 2004;279:42648–57. [PubMed: 15292216]
39. Kumar MS, Reddy PY, Kumar PA, Surolia I, Reddy GB. Effect of dicarbonyl-induced browning on alpha-crystallin chaperone-like activity: physiological significance and caveats of in vitro aggregation assays. Biochem J 2004;379:273–82. [PubMed: 14711370]
40. Pasta SY, Raman B, Ramakrishna T, Rao Ch M. Role of the conserved SRLFDQFFG region of alpha-crystallin, a small heat shock protein. Effect on oligomeric size, subunit exchange, and chaperone-like activity. J Biol Chem 2003;278:51159–66. [PubMed: 14532291]
41. Wyatt PJ. Light scattering and the absolute characterization of macromolecules. Anal Chim Acta 1993;272:1–40.
42. Pasta SY, Raman B, Ramakrishna T, Rao Ch M. The IXI/V motif in the C-terminal extension of alpha-crystallins: alternative interactions and oligomeric assemblies. Mol Vis 2004;10:655–62. [PubMed: 15448619]
43. Liao JH, Lee JS, Chiou SH. Distinct roles of alphaA- and alphaB-crystallins under thermal and UV stresses. Biochem Biophys Res Commun 2002;295:854–61. [PubMed: 12127973]
44. Bera S, Thampi P, Cho WJ, Abraham EC. A positive charge preservation at position 116 of alpha A-crystallin is critical for its structural and functional integrity. Biochemistry 2002;41:12421–6. [PubMed: 12369832]
45. Bova MP, Yaron O, Huang Q, Ding L, Haley DA, Stewart PL, Horwitz J. Mutation R120G in alphaB-crystallin, which is linked to a desmin-related myopathy, results in an irregular structure and defective chaperone-like function. Proc Natl Acad Sci U S A 1999;96:6137–42. [PubMed: 10339554]
46. Sun TX, Das BK, Liang JJ. Conformational and functional differences between recombinant human lens alphaA- and alphaB-crystallin. J Biol Chem 1997;272:6220–5. [PubMed: 9045637]
47. Reddy GB, Das KP, Petrash JM, Surewicz WK. Temperature-dependent chaperone activity and structural properties of human alphaA- and alphaB-crystallins. J Biol Chem 2000;275:4565–70. [PubMed: 10671481]
48. Das KP, Surewicz WK. Temperature-induced exposure of hydrophobic surfaces and its effect on the chaperone activity of alpha-crystallin. FEBS Lett 1995;369:321–5. [PubMed: 7649280]

49. Saha S, Das KP. Relationship between chaperone activity and oligomeric size of recombinant human alphaA- and alphaB-crystallin: a tryptic digestion study. Proteins 2004;57:610–7. [PubMed: 15382236]
50. Raman B, Ramakrishna T, Rao CM. Temperature dependent chaperone-like activity of alpha-crystallin. FEBS Lett 1995;365:133–6. [PubMed: 7781765]
51. Bhattacharyya J, Srinivas V, Sharma KK. Evaluation of hydrophobicity versus chaperonelike activity of bovine alphaA- and alphaB-crystallin. J Protein Chem 2002;21:65–71. [PubMed: 11902669]
52. Kumar MS, Kapoor M, Sinha S, Reddy GB. Insights into hydrophobicity and the chaperone-like function of alphaA- and alphaB-crystallins: an isothermal titration calorimetric study. J Biol Chem 2005;280:21726–30. [PubMed: 15817465]
53. McClure WO, Edelman GM. Fluorescent probes for conformational states of proteins. I. Mechanism of fluorescence of 2-p-toluidinylnaphthalene-6-sulfonate, a hydrophobic probe. Biochemistry 1966;5:1908–19. [PubMed: 4164420]
54. Shroff NP, Bera S, Cherian-Shaw M, Abraham EC. Substituted hydrophobic and hydrophilic residues at methionine-68 influence the chaperone-like function of alphaB-crystallin. Mol Cell Biochem 2001;220:127–33. [PubMed: 11451372]
55. Rawat U, Rao M. Interactions of chaperone alpha-crystallin with the molten globule state of xylose reductase. Implications for reconstitution of the active enzyme. J Biol Chem 1998;273:9415–23. [PubMed: 9545266]
56. Wang K, Spector A. The chaperone activity of bovine alpha crystallin. Interaction with other lens crystallins in native and denatured states. J Biol Chem 1994;269:13601–8. [PubMed: 7909809]
57. Wang K, Spector A. alpha-crystallin prevents irreversible protein denaturation and acts cooperatively with other heat-shock proteins to renature the stabilized partially denatured protein in an ATP-dependent manner. Eur J Biochem 2000;267:4705–12. [PubMed: 10903503]
58. Muchowski PJ, Clark JI. ATP-enhanced molecular chaperone functions of the small heat shock protein human alphaB crystallin. Proc Natl Acad Sci U S A 1998;95:1004–9. [PubMed: 9448275]
59. Clark JI, Estrada MR, Ghosh JG. Interaction sites in human alphaB-crystallin mediate multiple functions. Invest Ophthalmol Visual Sci 2004;45E-abstract 3976

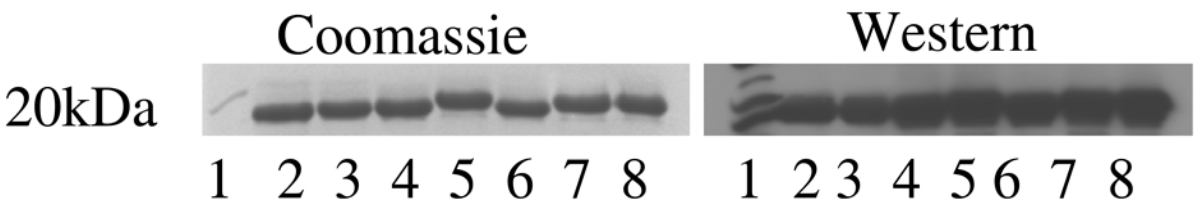

Fig 1. Purification of human recombinantαA-crystallin

Four μg protein was subjected to SDS-PAGE on a 12% reducing gel, then either stained with Coomassie blue (Panel A) or Western blotted using a rabbit polyclonal antibody to human αA/αB-crystallin (Panel B). 1, molecular weight markers; 2, wt αA-crystallin; 3, R21A; 4, R49A; 5, R103A; 6, R21A/R49A; 7, R21A/R103A; 8, R21A/R49A/R103A.

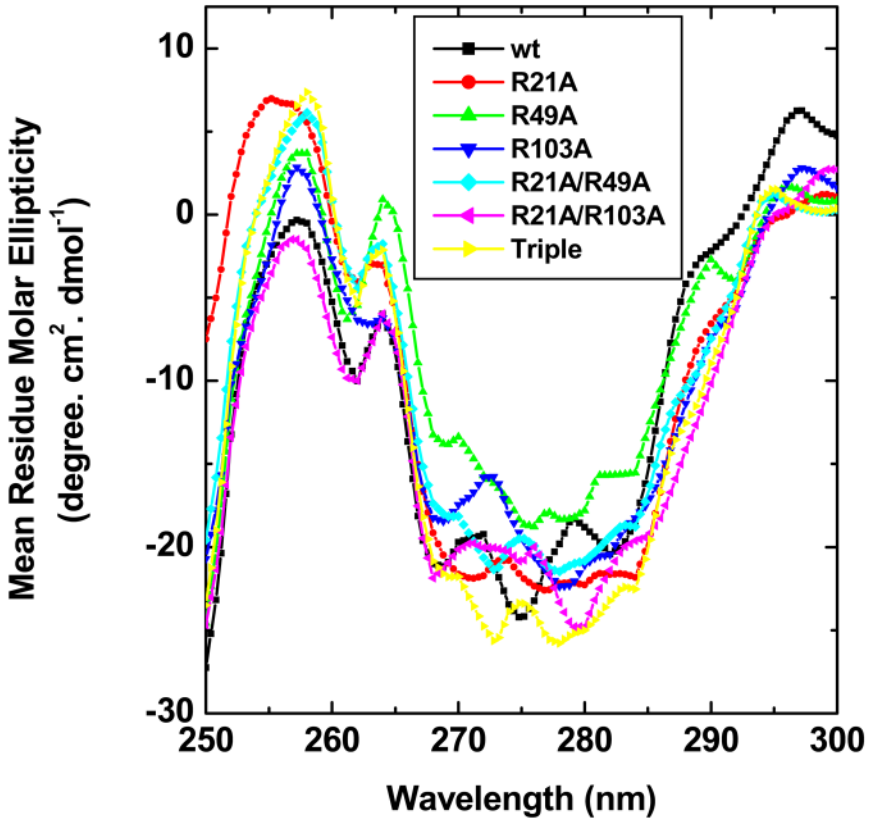

Fig 2. Near UV circular dichroic spectra of humanαA-crystallin

Proteins (1.0 mg/ml) were in 10 mM phosphate buffer (pH 7.2) at 25 °C. Spectra were measured in a 10 mm path length CD quartz cell. Data were collected at 0.4 nm wavelength resolution.

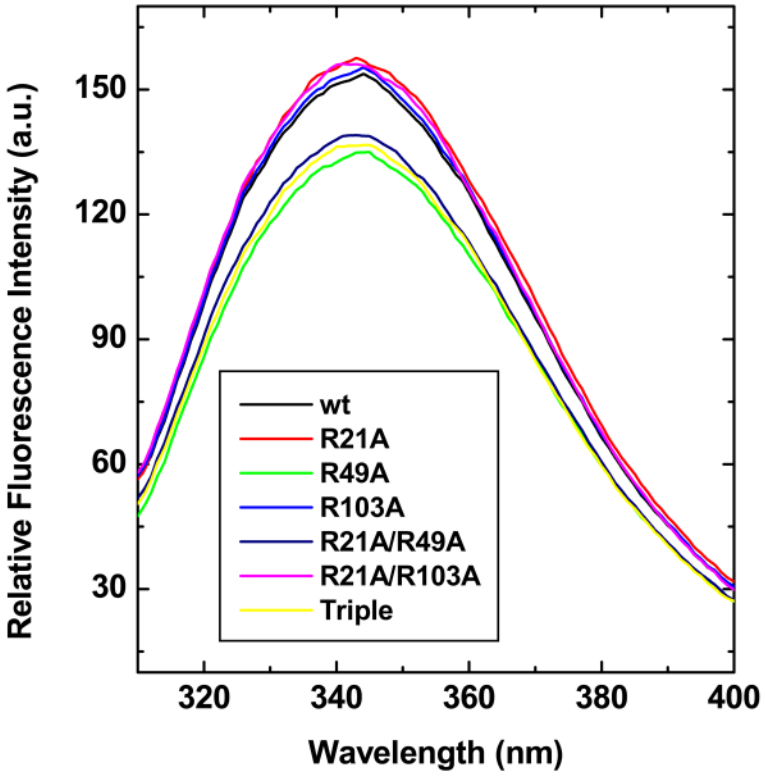

Fig 3. Intrinsic fluorescence spectra of humanαA-crystallin

The fluorescence spectrum of different samples (0.1 mg/ml protein) was recorded from 310–400 nm at 25 °C. The excitation wavelength was 295 nm. Data were collected at 0.5 nm wavelength resolution.

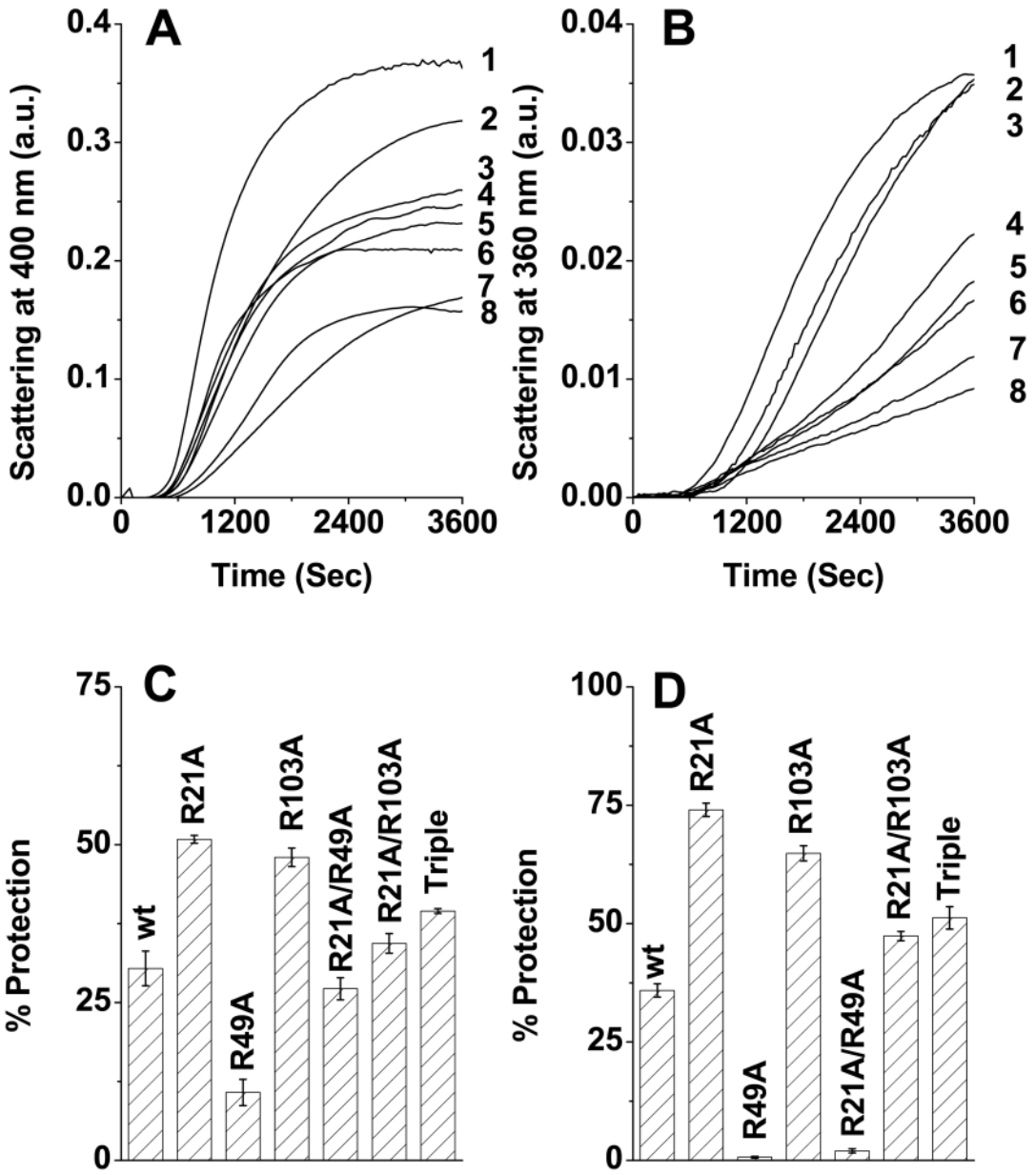

Fig 4. Chaperone function of humanαA-crystallin

DTT induced aggregation of 0.32 mg/ml insulin at 25 °C (Panel A) and thermal aggregation of 0.06 mg/ml CS at 43 °C (Panel B) in the presence or absence of different αA-crystallin preparations. Trace 1 = target protein (TP) alone; trace 2 = TP + R49A; trace 3 = TP +R21A/R49A; trace 4 = TP + wt; trace 5 = TP +R21A/R103A; trace 6 = TP +Triple (R21A/R49A/R103A) ; trace 7 = TP + R103A; trace 8 = TP +R21A. Panels C and D show the percent protection ability of different αA-crystallin against insulin- and CS aggregation. The chaperone: substrate ratio (w/w) was 1:5 and 1:15 for insulin and CS aggregation assays. Data are means ± standard deviation from triplicate determinations.

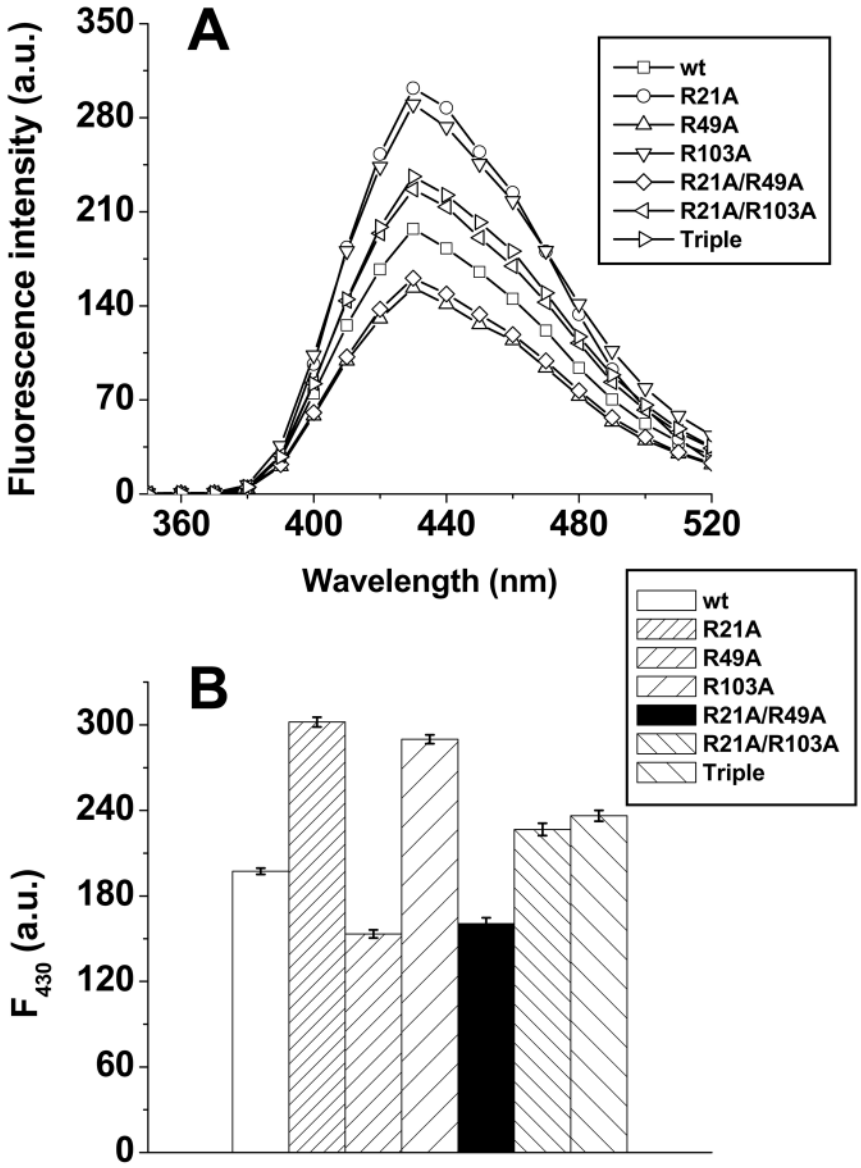

Fig 5. A) Fluorescence spectra of TNS boundαA-crystallin

Protein concentration was 0.1 mg/ml and TNS concentration was 100 μM. The fluorescence spectrum of different samples at 25 °C was recorded from 350–520 nm. The excitation wavelength was 320 nm. **B)** Fluorescence intensity at 430 nm (emission maxima) for wt and mutant αA-crystallin at 25 °C.

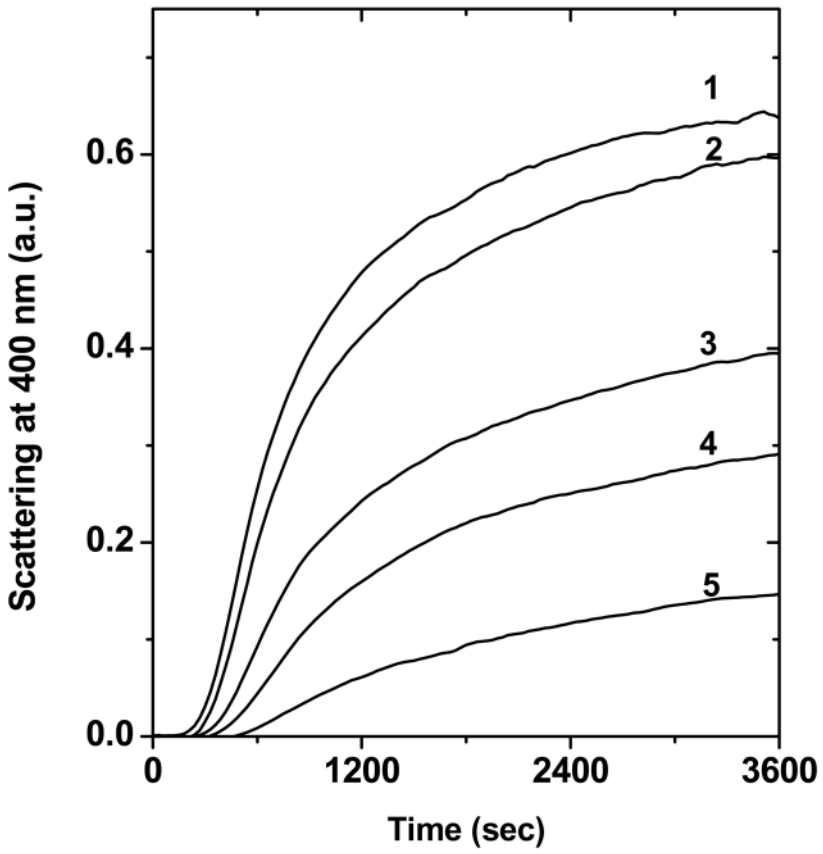

Fig 6. Inhibition of thermal aggregation of carbonic anhydrase (CA)

CA was incubated at 60 °C for 1 hr in 50 mM phosphate buffer (pH 7.2) containing 100 mM NaCl in the presence or absence of indicated proteins. Light scattering due to protein aggregation was monitored at 400 nm. Trace 1 = 0.24 mg/ml CA alone; trace 2 = CA + 0.06 mg/ml R49A; trace 3 = CA +0.06 mg/ml wt; trace 4 = CA +0.06 mg/ml R103A; trace 5 = CA + 0.06 mg/ml R21A.

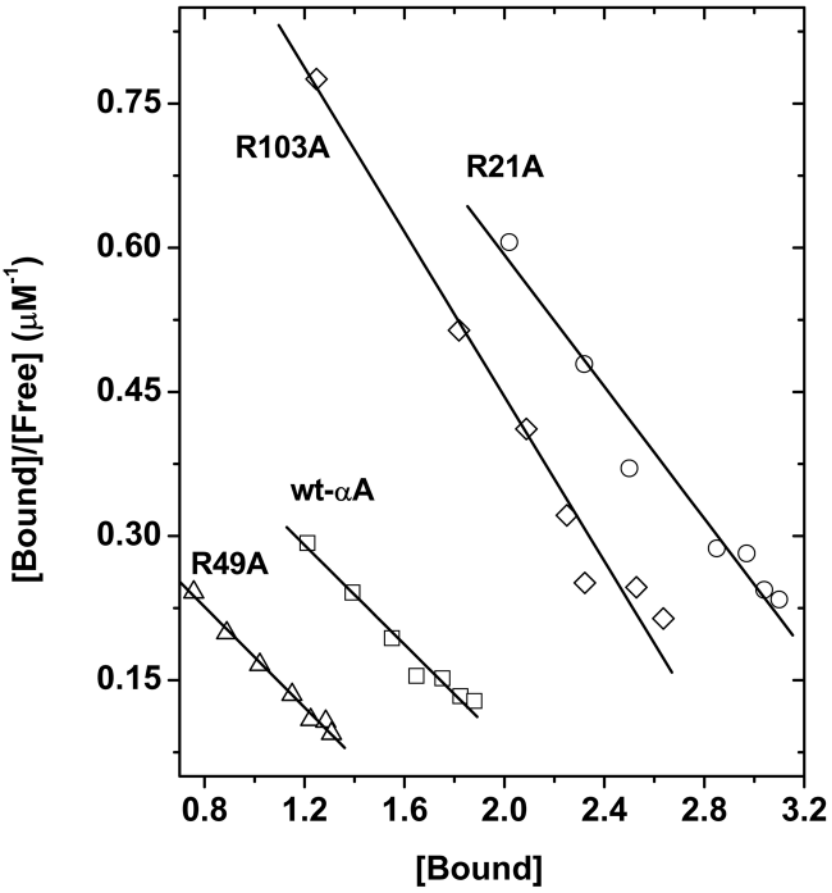

Fig 7. Binding constant of αA-crystallin for carbonic anhydrase

Scatchard plot to calculate binding parameters for the interaction between CA and different recombinant α A-crystallins at 60 °C.

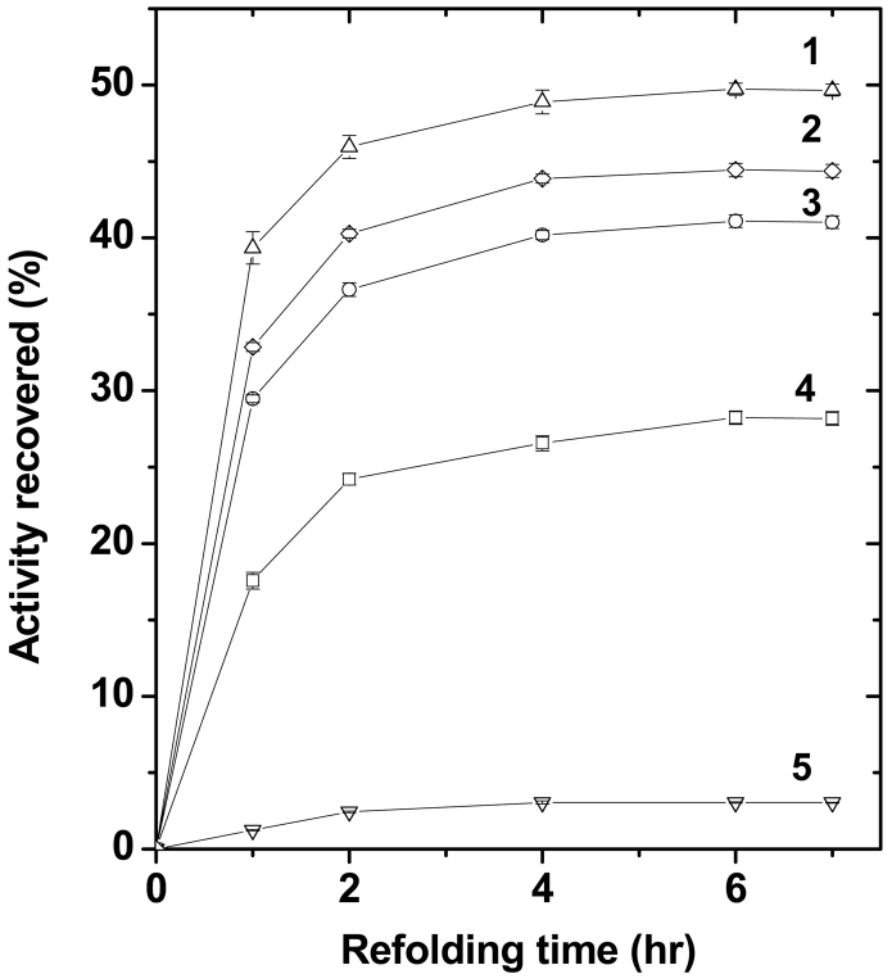

Fig 8. Reactivation of malate dehydrogenase (MDH) byαA-crystallin

MDH was inactivated by incubation at 25°C in 6M Gu-HCl solution. Trace 5 = 10 nM MDH alone; trace 4 = 10 nM MDH + 30 μM R49A; trace 3 = 10 nM MDH + 30 μM wt; trace 2 = 10 nM MDH + 30 μM R103A; trace 1 = 10 nM MDH + 30 μM R21A. Refolding was initiated by 100-fold dilution of MDH (1 μM) in 6M Gu-HCl in refolding buffer (pH 7.5) containing 50 mM phosphate, 10 mM Mg-acetate and 5 mM DTT. Each data point is the average of triplicate measurement and error bars denote standard deviation.

Table 1

Oligonucleotide primers used for site directed mutagenesis of human αA-crystallin

Protein	Template	Primers
N-terminal His Tag	wt αA	(*)
R21A	wt αA	FP; 5′-TTCTACCCCAGCGCGCTGTTCGACCAG-3′
		RP (*)
R49A	His Tag	FP : His-tag forward primer (*)
	wt αA	RP: 5′-GAGGGACTGGGCGTAGTAGGG-3′
R103A	His Tag	FP: 5′-CACAACGAGGCCCAGGACGAC-3′
	wt αA	RP: His-tag reverse primer (*)
R21A/R49A	His Tag	FP : His-tag forward primer (*)
	R21AαA	RP: 5′-GAGGGACTGGGCGTAGTAGGG-3′
R21A/R103A	His Tag	FP: 5′-CACAACGAGGCCCAGGACGAC-3′
	R21AαA	RP: His-tag reverse primer (*)
R21A/R49A/R103A	His Tag	FP: 5′-CACAACGAGGCCCAGGACGAC-3′
	R21AαA	RP: 5′-GAGGGACTGGGCGTAGTAGGG-3′

* See experimental procedures

Table 2

Molar mass, polydispersity index and hydrodynamic radii (R_h) of wild type and mutant human αA-crystallin determined by dynamic light scattering

Proteins	Molar mass distribution (g/mol)	Average molar mass (g/mol, M_w)	Polydispersity Index (PDI)	Hydrodynamic radii (R_h) (nm)
wt	$1.75e^6$–$1.96e^6$	$2.18e^6$	1.014	12.2
R21A	$1.76e^6$–$2.31e^6$	$1.93e^6$	1.002	11.8
R49A	$2.34e^6$–$1.87e^7$	$2.49e^6$	1.295	15.8
R103A	$2.75e^6$–$1.09e^7$	$3.10e^6$	1.250	16.9
R21A/R49A	$1.99e^6$–$4.11e^6$	$2.51e^6$	1.016	12.8
R21A/R103A	$1.36e^6$–$5.37e^6$	$1.97e^6$	1.140	14.0
R21A/R49A/R103A	$2.36e^6$–$1.16e^7$	$2.99e^6$	1.202	15.5

Table 3

Percent levels of secondary structure in αA-wt protein and its mutants using CONTINLL software

	wt	R21A	R49A	R103A	R21A/R49A	R21A/R103A	Triple
α-helix	5.7	5.3	5.8	7.4	6.9	7.5	6.9
β-sheet	38.8	40.9	38.2	38.7	39.1	38.0	39.1
β -turn	22.3	22.1	22.6	21.9	22.1	22.1	22.0
Random coil	33.1	31.7	33.6	32.0	32.0	32.3	32.1

Table 4

Determination of n and dissociation constant (K_d) values for the interaction of human αA-crystallin and its mutants with carbonic anhydrase (CA) at 60 °C

System studied	n	K_d (μM)
Human αA-crystallin + CA	2.32 ± 0.06	3.87 ± 0.30
R21A + CA	3.73 ± 0.09	2.92 ± 0.24
R49A + CA	1.67 ± 0.02	3.82 ± 0.15
R103A + CA	3.04 ± 0.07	2.33 ± 0.17